Supporting Information

Delineating the intricacies of niobium-modified high-nickel layered cathodes with a single-step synthesis

Thomas J. Watts and Arumugam Manthiram

Walker Department of Mechanical Engineering and Texas Materials Institute
The University of Texas at Austin
Austin, Texas 78712, United States

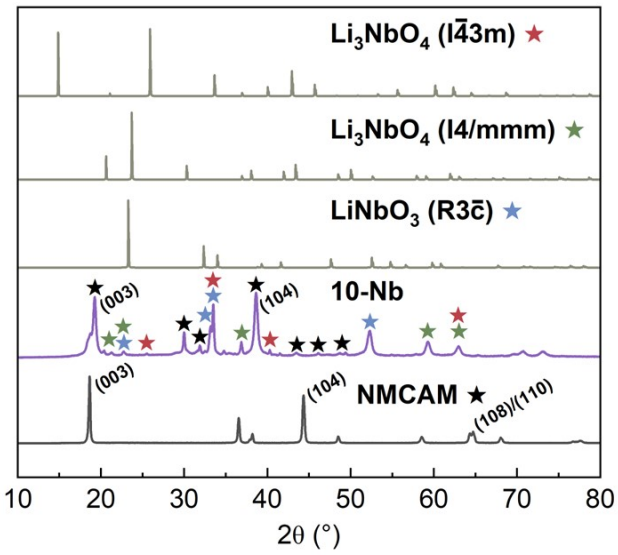

Figure S1. XRD analysis of the unmodified NMCAM and the 10-Nb sample compared to the calculated powder diffraction patterns of $LiNbO_3$ and Li_3NbO_4.

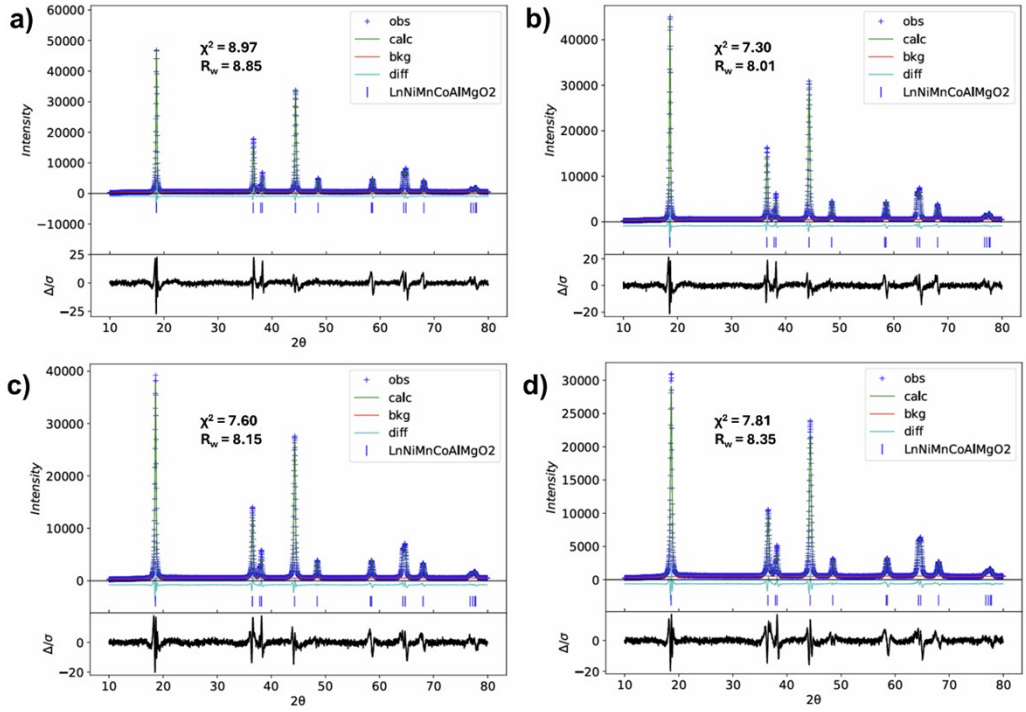

Figure S2. Rietveld refinement results for (a) NMCAM [1% ex LiOH], (b) 0.5-Nb [5.5% ex LiOH], (c) 1.0-Nb [7% ex LiOH], and (d) 2.0-Nb samples [10% ex LiOH].

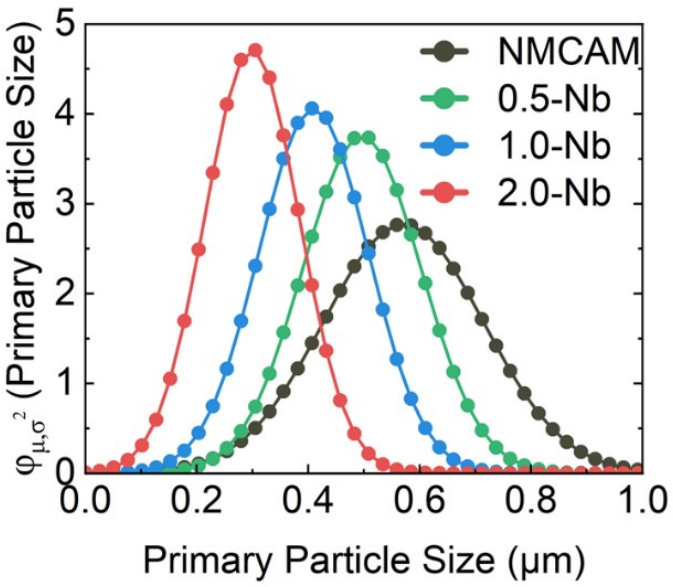

Figure S3. Distribution of primary particle size.

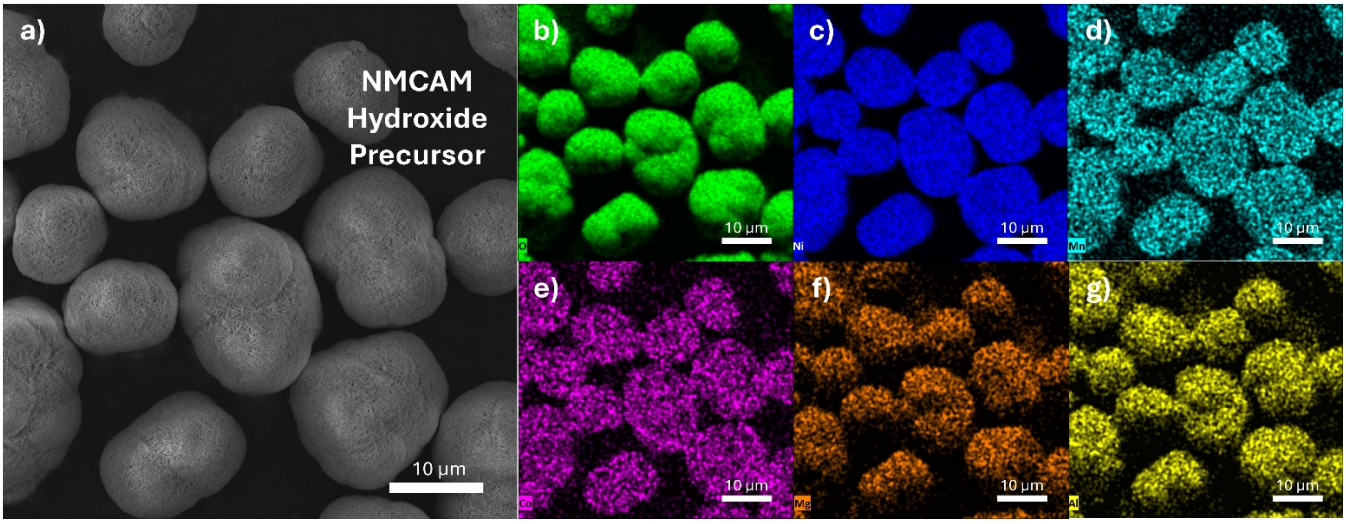

Figure S4. (a) SEM image of NMCAM hydroxide precursor. Elemental maps of the image for (b) oxygen, (c) nickel, (d) manganese, (e) cobalt, (f) magnesium, and (g) aluminum.

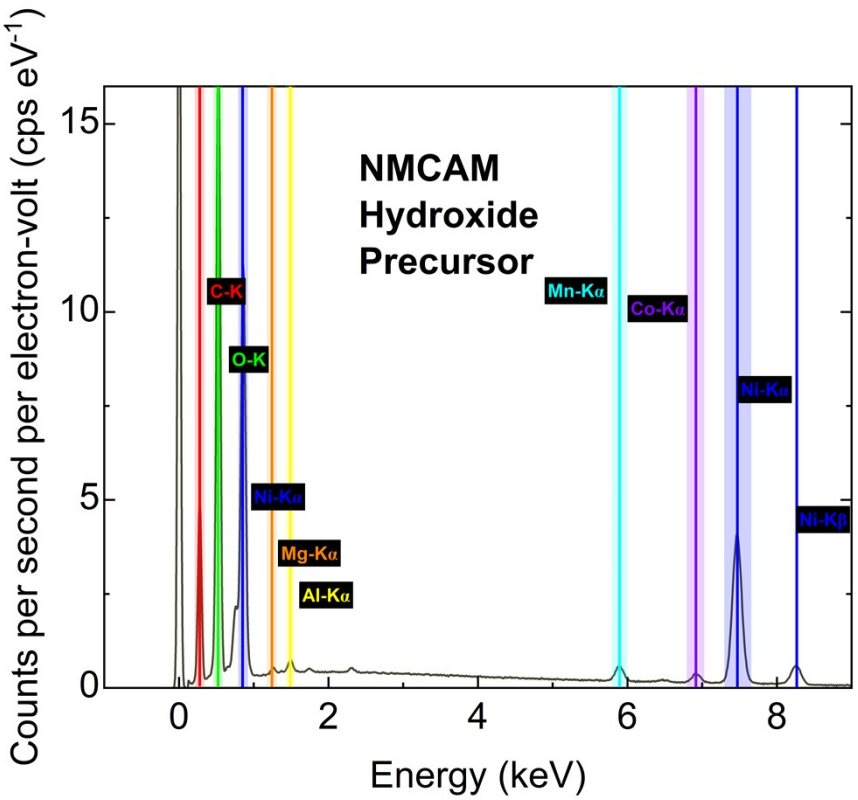

Figure S5. EDX spectra of NMCAM hydroxide precursor

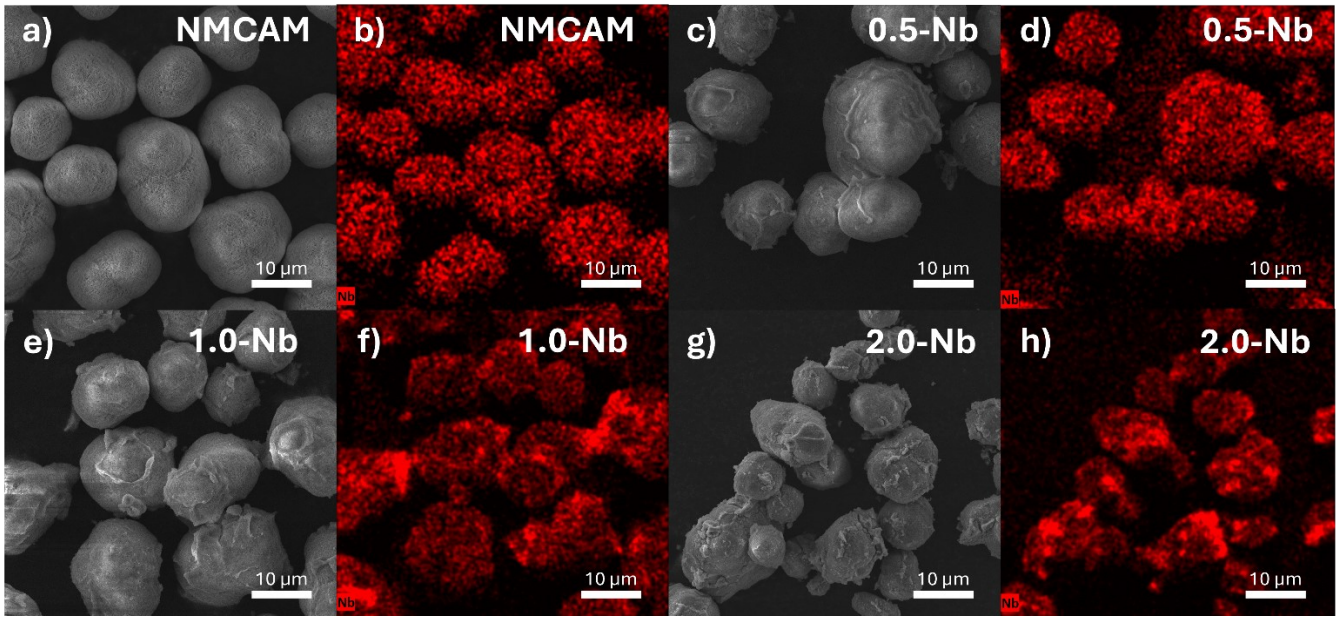

Figure S6. SEM image of hydroxide precursor and its corresponding Nb elemental map of (a) and (b) NMCAM, (c) and (d) 0.5-Nb, (e) and (f) 1.0-Nb, (g) and (h) 2.0-Nb samples.

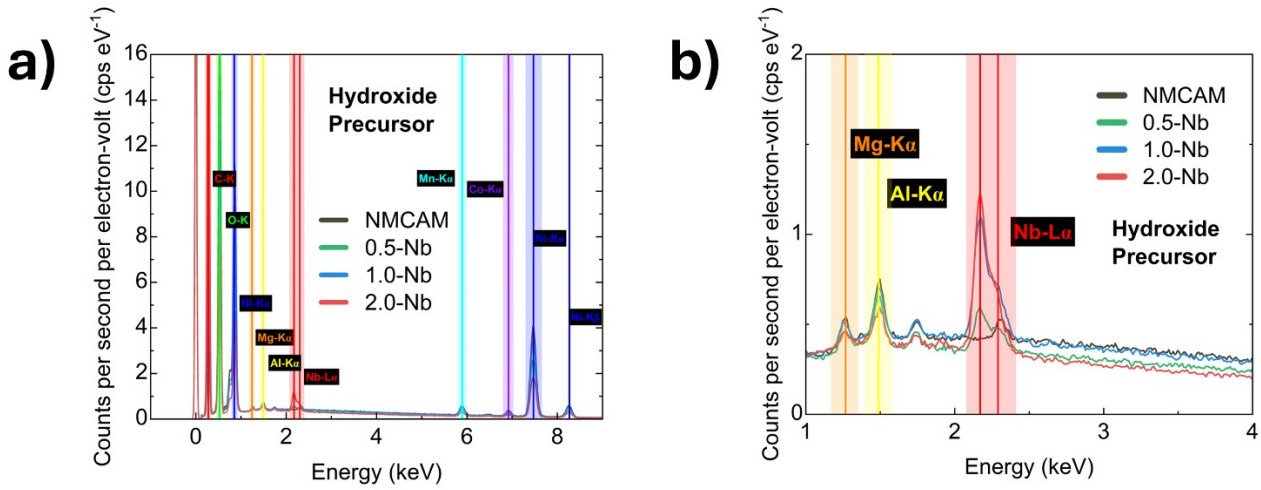

Figure S7. (a) EDX spectra of the hydroxide precursors after coating with ANO. (b) EDX spectra of the hydroxide precursors magnified to focus on the Mg-Kα, Al-Kα, and Nb-Lα peaks.

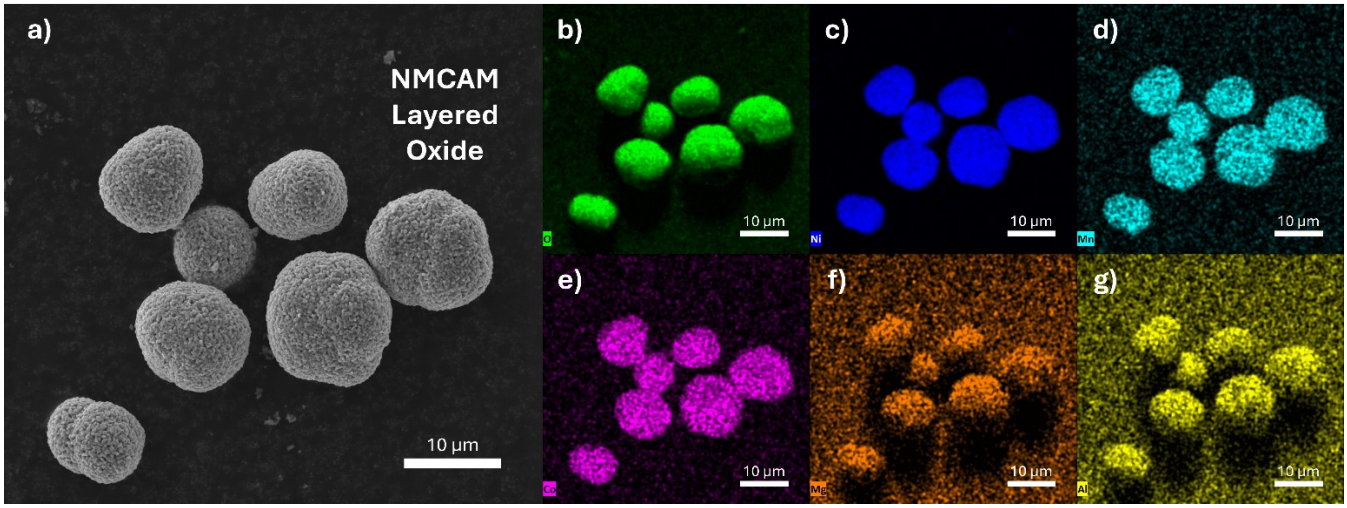

Figure S8. (a) SEM image of NMCAM layered oxide. Elemental maps of the image for (b) oxygen, (c) nickel, (d) manganese, (e) cobalt, (f) magnesium, and (g) aluminum.

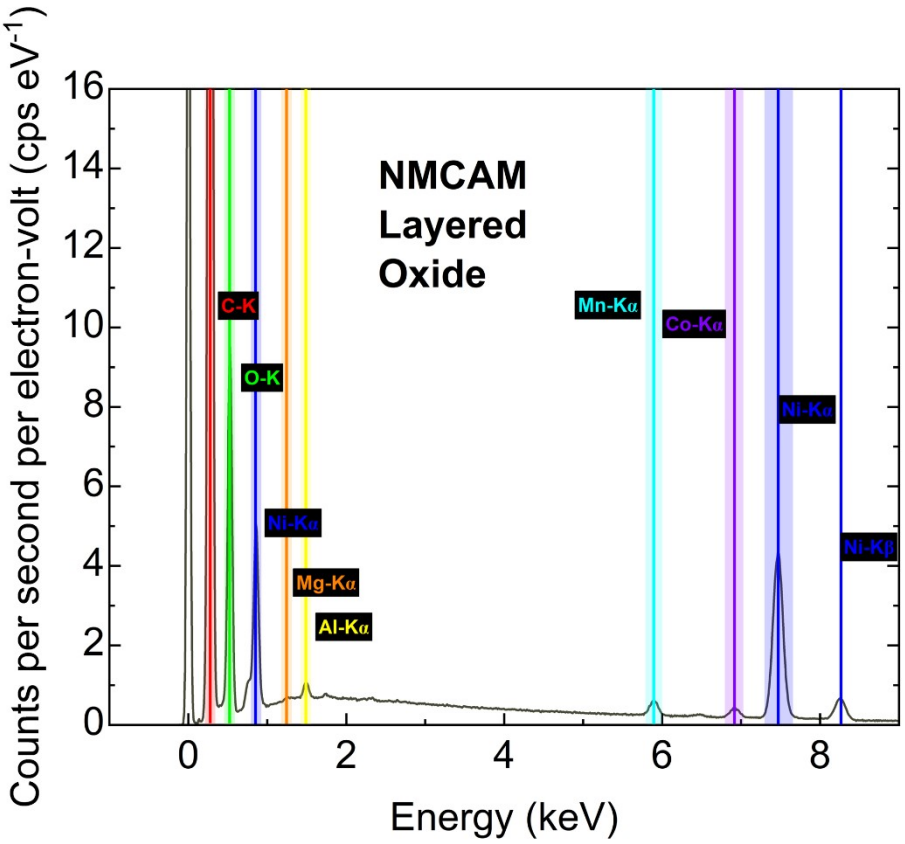

Figure S9. EDX spectra of NMCAM layered oxide

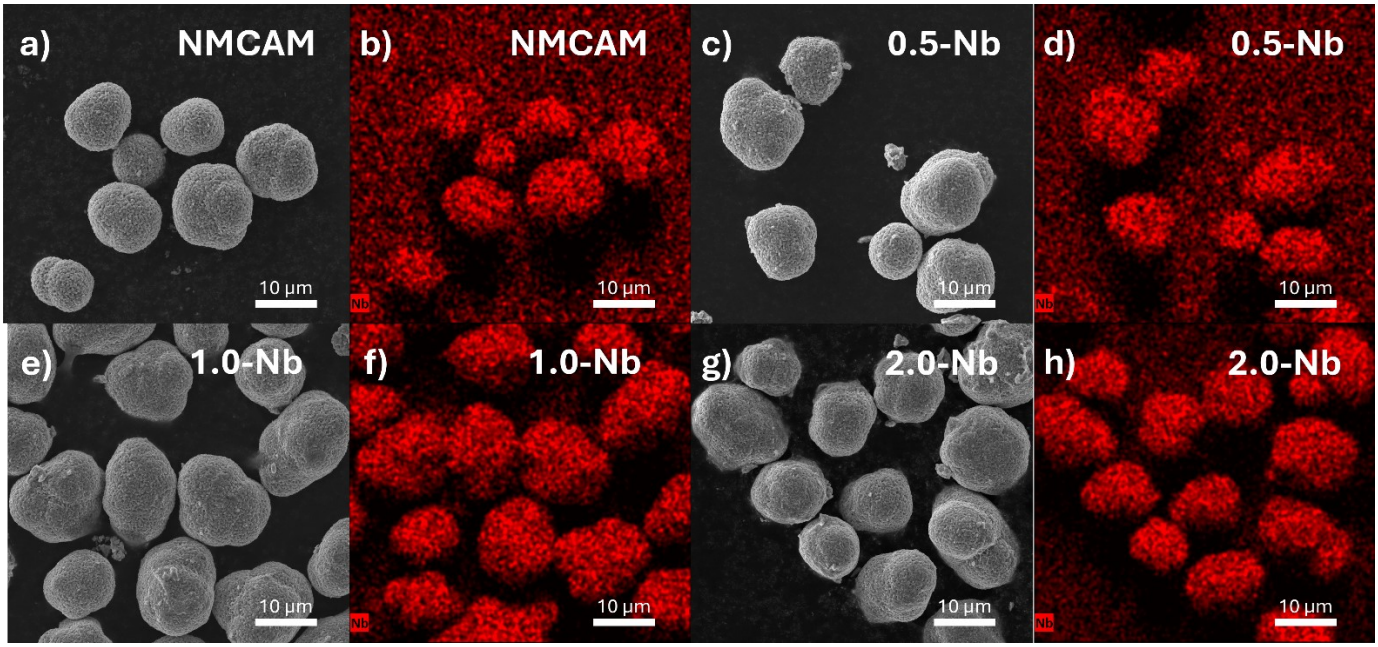

Figure S10. SEM image of layered oxide particles and its corresponding Nb elemental map of (a) and (b) NMCAM, (c) and (d) 0.5-Nb, (e) and (f) 1.0-Nb, (g) and (h) 2.0-Nb samples.

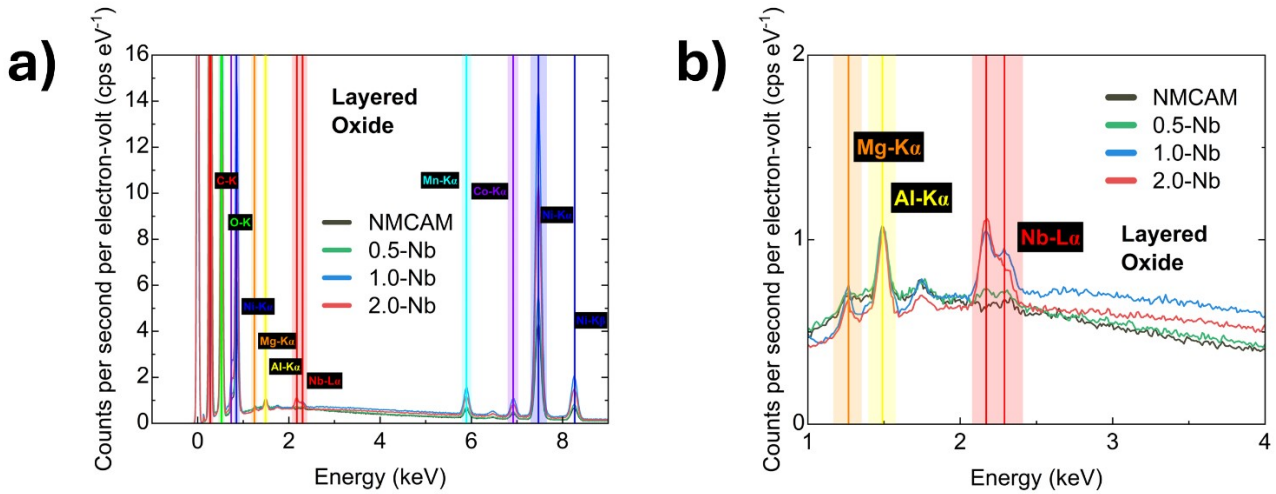

Figure S11. (a) EDX spectra of the layered oxide samples after coating with ANO. (b) EDX spectra of the layered oxide samples magnified to focus on the Mg-Kα, Al-Kα, and Nb-Lα peaks.

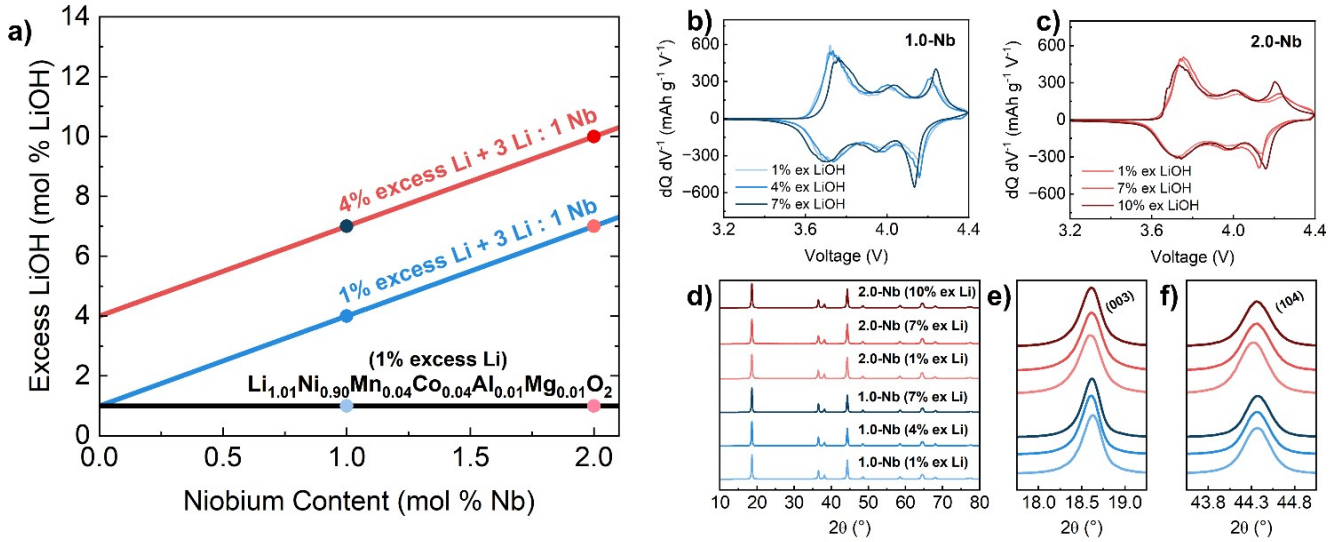

Figure S12. (a) Variation of excess LiOH ratio vs. Nb content. dQ dV^{-1} vs. voltage plots at C/3 rate of (b) 1.0-Nb and (c) 2.0-Nb samples. (d) Full XRD patterns of 1.0-Nb and 2.0-Nb samples with various excess LiOH contents and (e) (003) peak and (f) (104) peak magnified over a narrow 2θ range.

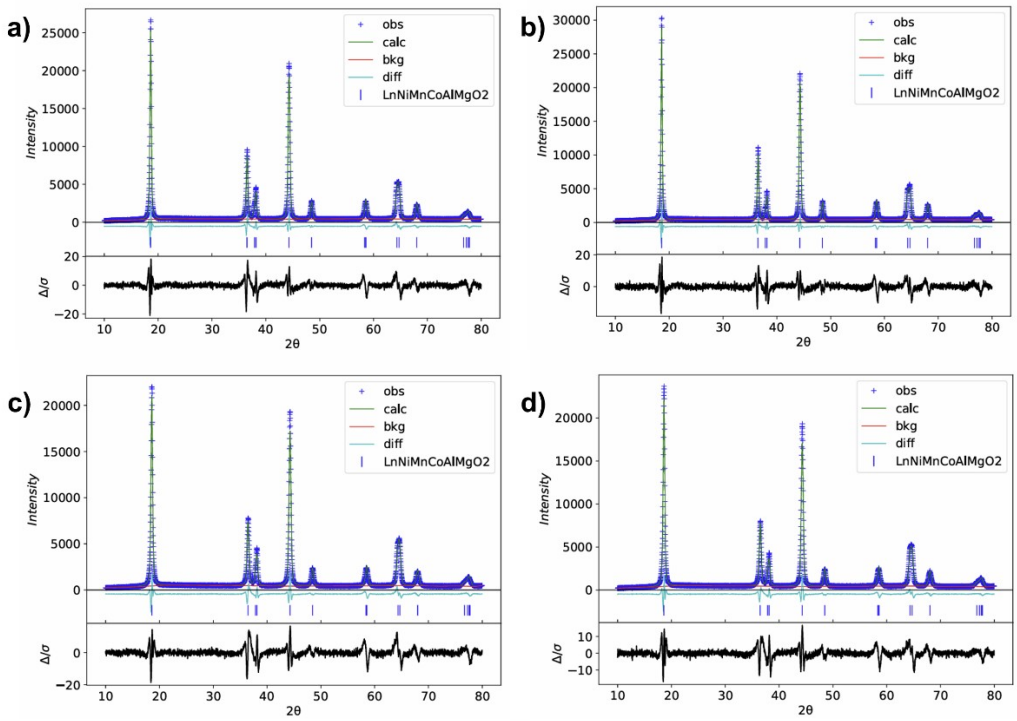

Figure S13. Rietveld refinement results for (a) 1.0-Nb [1% ex LiOH], (b) 1.0-Nb [4% ex LiOH], (c) 2.0-Nb [1% ex LiOH], and (d) 2.0-Nb [7% ex LiOH].

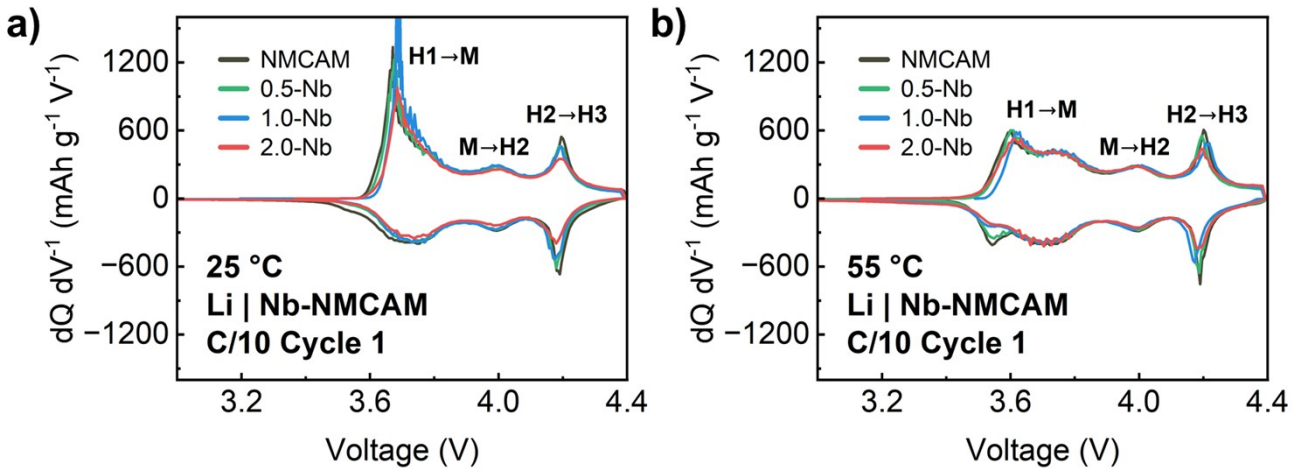

Figure S14. dQ dV^{-1} vs. voltage plots for half cells during the initial C/10 formation cycle at (a) 25 °C, and (b) 55 °C.

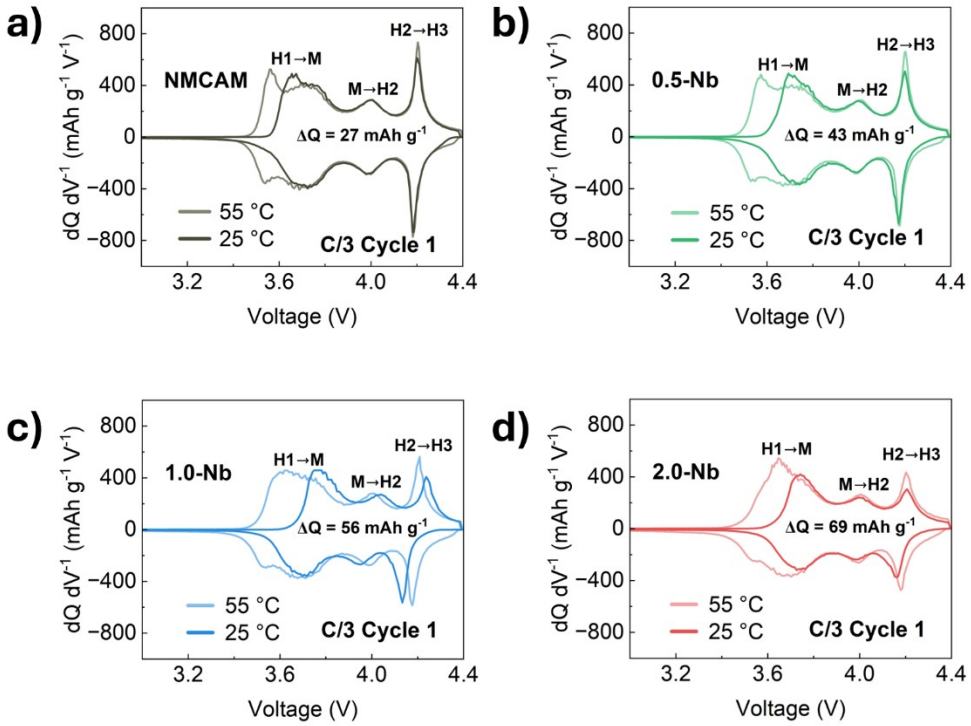

Figure S15. dQ dV^{-1} vs. voltage plots depicting the origins of room-temperature capacity loss for (a) NMCAM, (b) 0.5-Nb, (c) 1.0-Nb, and (d) 2.0-Nb samples.

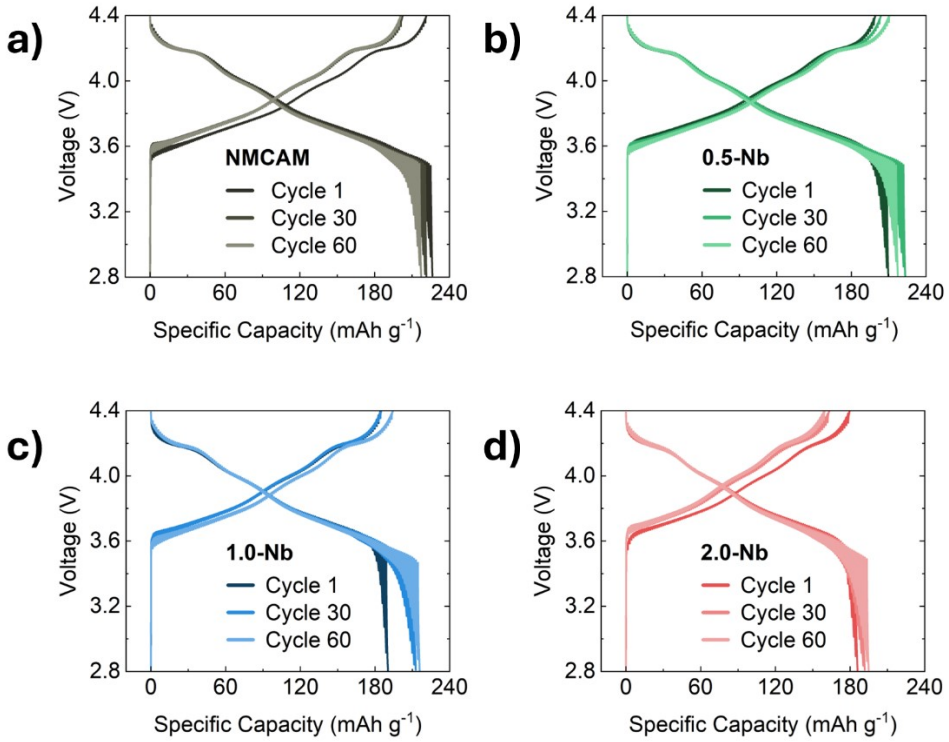

Figure S16. Voltage vs. specific capacity plots of GITT cycles for (a) NMCAM, (b) 0.5-Nb, (c) 1.0-Nb, and (d) 2.0-Nb samples.

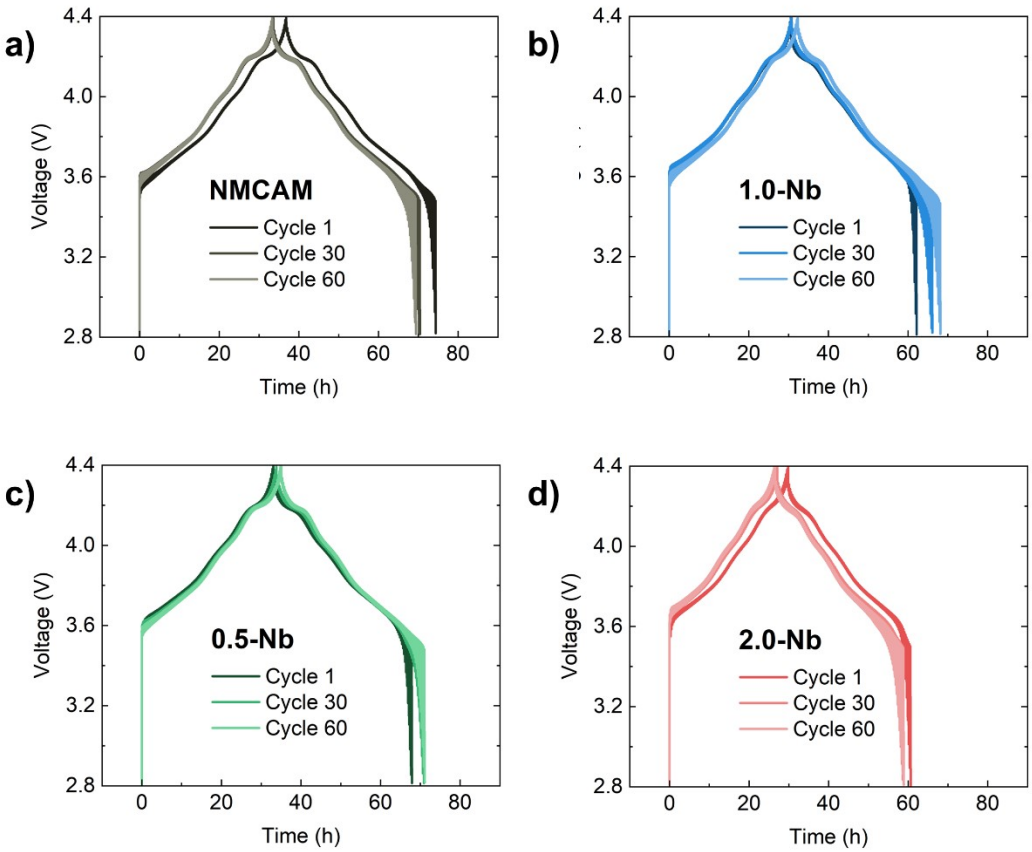

Figure S17. Voltage vs. specific capacity plots of GITT cycles for (a) NMCAM, (b) 0.5-Nb, (c) 1.0-Nb, and (d) 2.0-Nb samples.

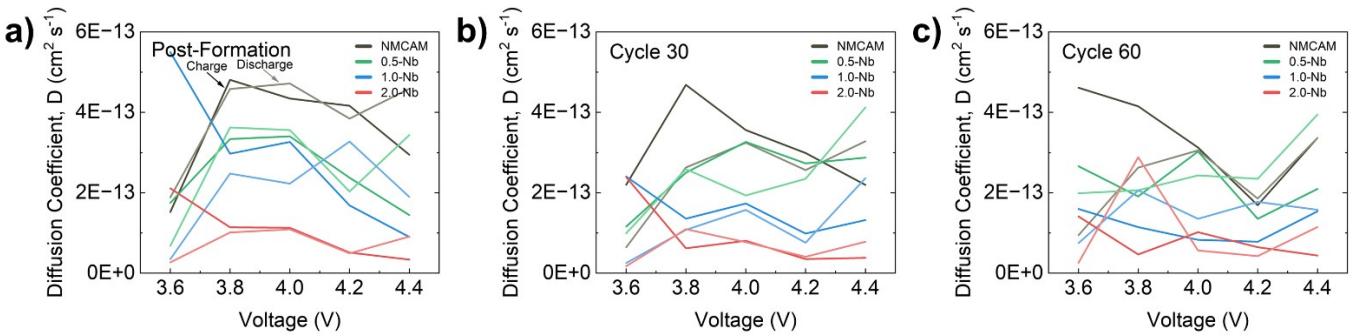

Figure S18. Li^+ diffusion coefficient vs. voltage plots for Nb-modified NMCAM samples after (a) formation cycling, (b) 30 C/3 cycles, and (c) 60 C/3 cycles.

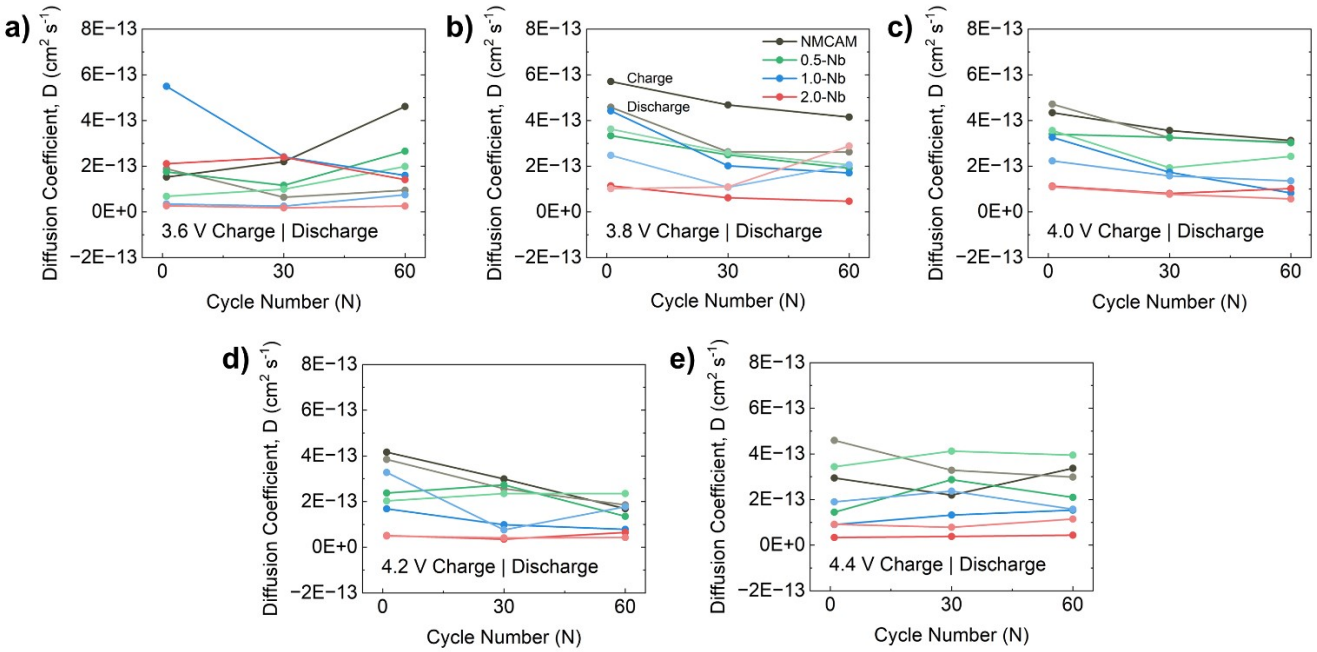

Figure S19. Li^+ diffusion coefficient vs. cycle number for Nb-modified NMCAM samples at (a) 3.6 V, (b) 3.8 V, (c) 4.0 V, (d) 4.2 V, (e) 4.4 V.

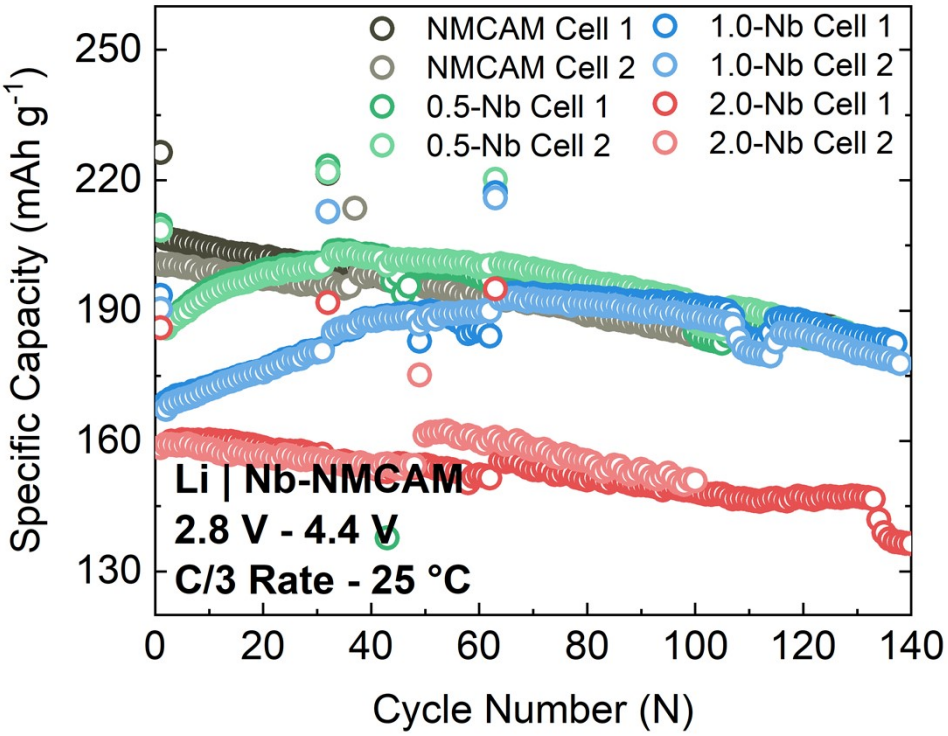

Figure S20. Specific capacity vs. cycle number plots of Nb-modified half cells, with GITT measured after the formation cycles (included in the plot) and at C/3 rate at cycles 30 and 60 (cycle numbers 34 and 64 in the plot).

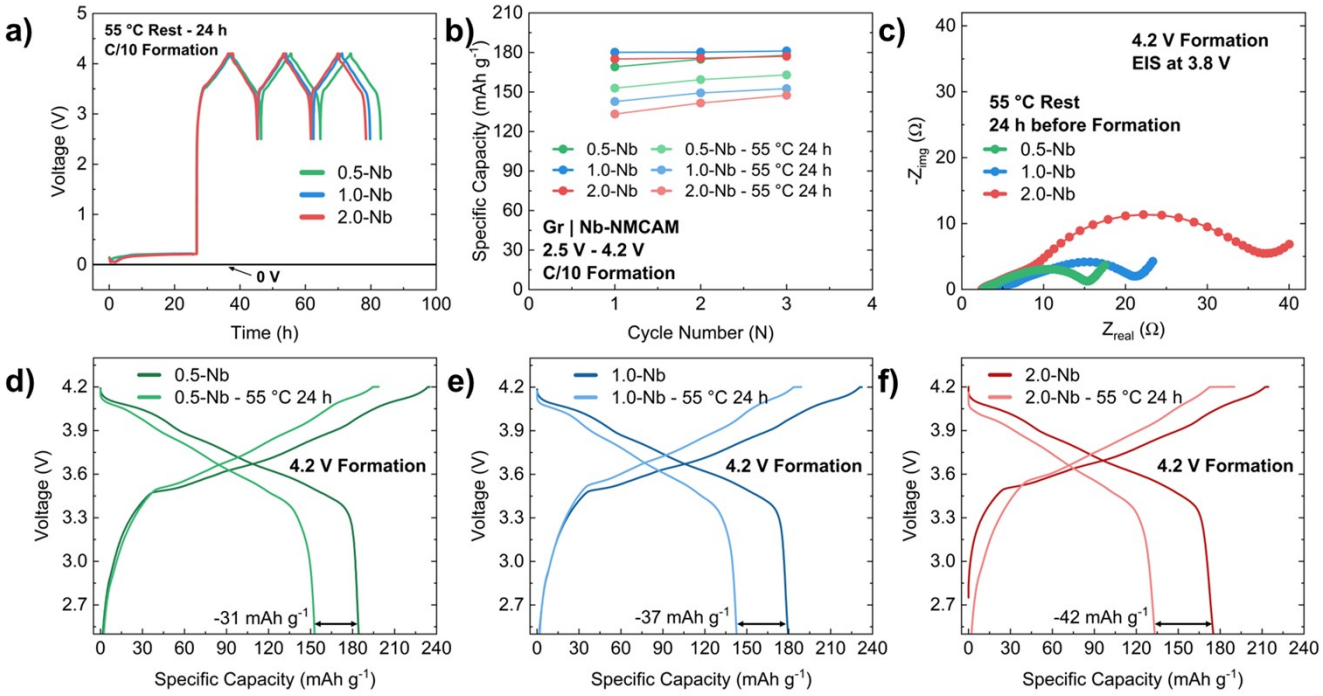

Figure S21. Electrochemical performance of coin full cells cycled at room temperature after a 24 h rest at 55 °C after cell assembly. (a) Voltage vs. time including 24 h rest, (b) Specific capacity vs. cycle number for formation cycles. (c) Nyquist plot of all full cells charged to 3.8 V after formation. Voltage vs. specific capacity plots of the first C/10 formation cycle of cells experiencing the 55 °C rest and those without the 55 °C rest for (d) 0.5-Nb, (e) 1.0-Nb, and (f) 2.0-Nb.

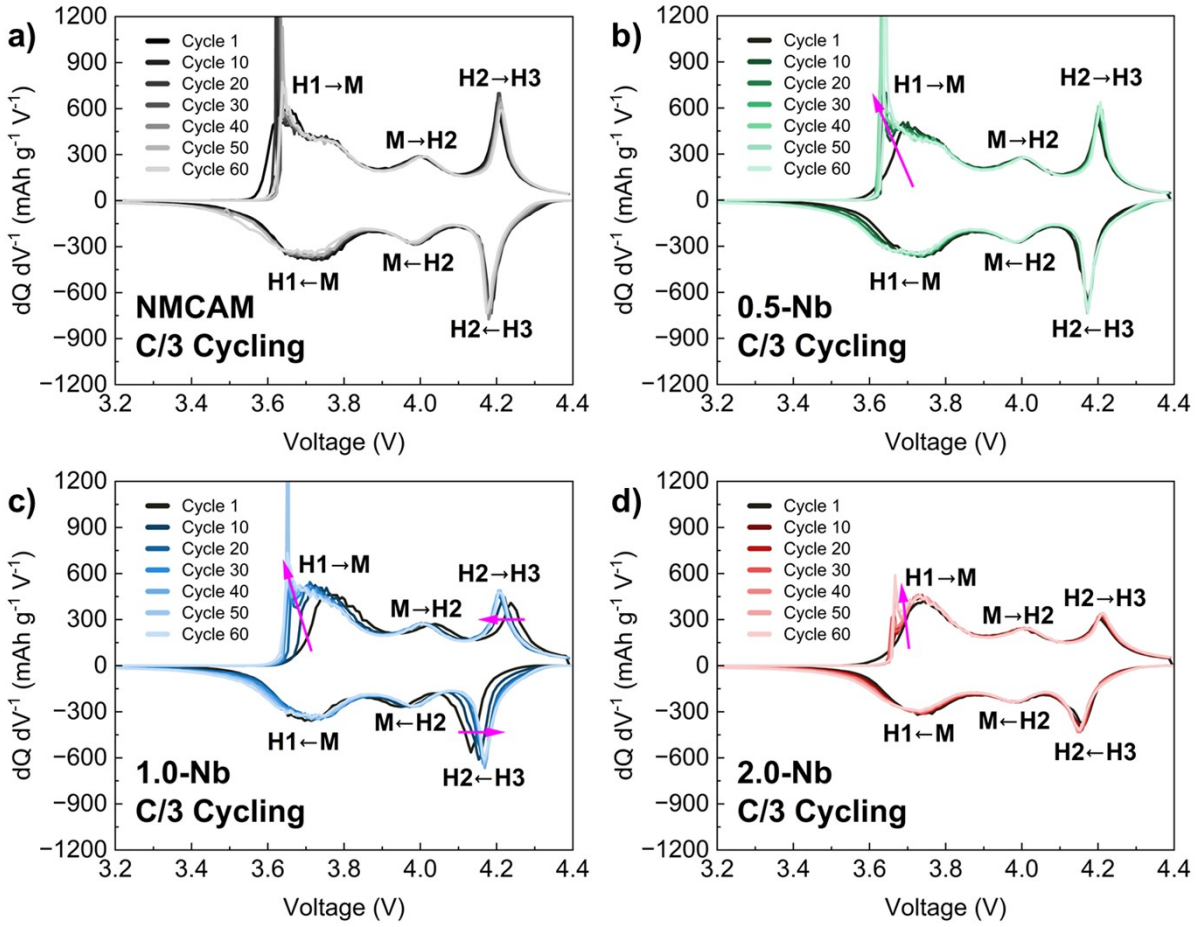

Figure S22. dQ dV^{-1} vs voltage plots for (a) NMCAM, (b) 0.5-Nb, (c) 1.0-Nb, and (d) 2.0-Nb after formation, and at C/3 cycle number 10, 20, 30, 40, 50, and 60.

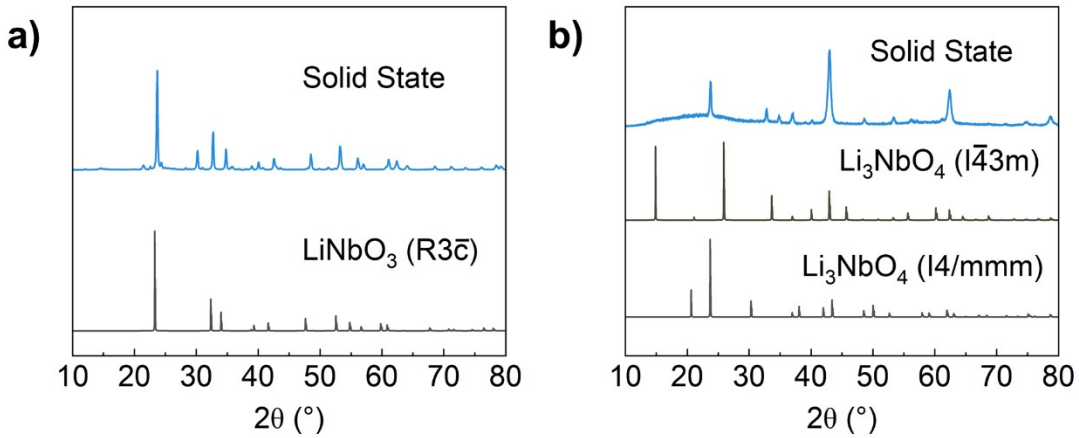

Figure S23. XRD analysis of (a) $LiNbO_3$ and (b) Li_3NbO_4 compared to calculated powder diffraction patterns of matching phases.

Figure S24. Images of cell components utilized to measure the electronic conductivities of lithium niobate powders, and the assembled cell.

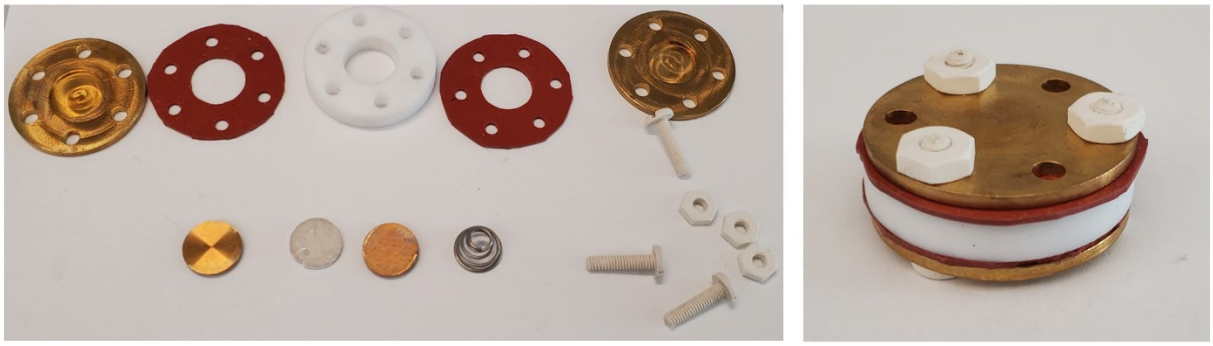

Figure S25. Images of cell components utilized to measure the ionic conductivities of lithium niobate powders, and the assembled cell.

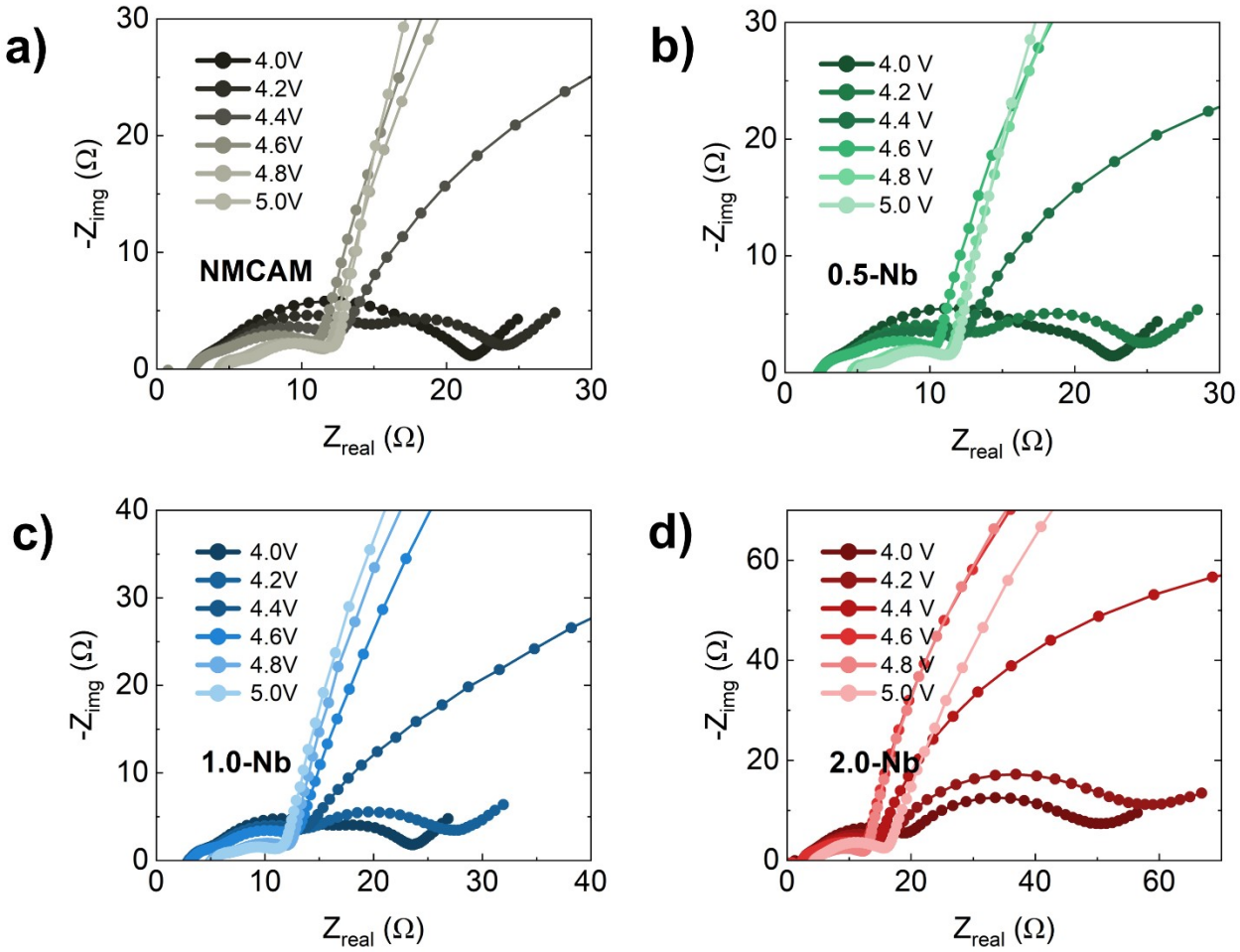

Figure S26. Nyquist plots of (g) NMCAM, (h) 0.5-Nb, (i) 1.0-Nb, (j) 2.0-Nb samples. EIS was collected during formation cycling to 5.0 V every 200 mV.

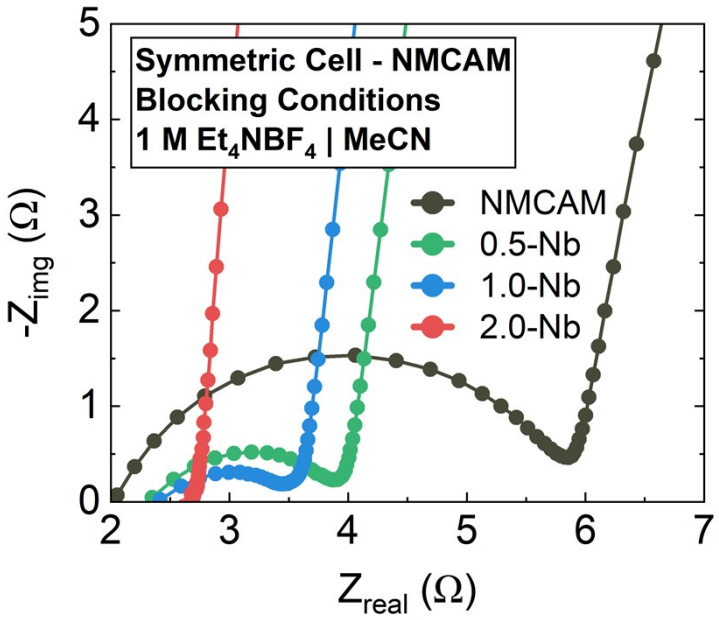

Figure S27. Nyquist plots of NMCAM and Nb-modified NMCAM symmetric cells under blocking conditions at room temperature.

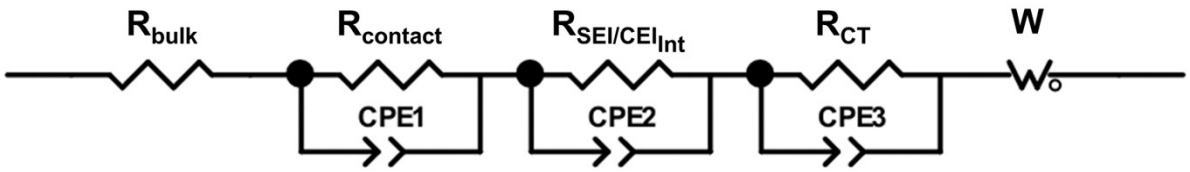

Figure S28. EIS Equivalent-circuit model.

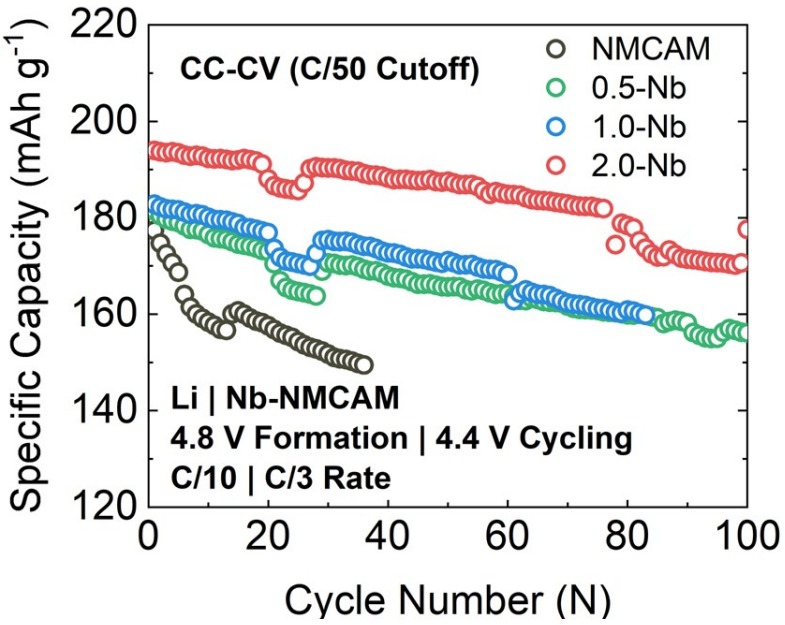

Figure S29. Electrochemical performanced of Nb-NMCAM samples cycled under a 4.8 V CC-CV formation at a C/50 cutoff, followed by C/3 rate cycling at 4.4 V cutoff.

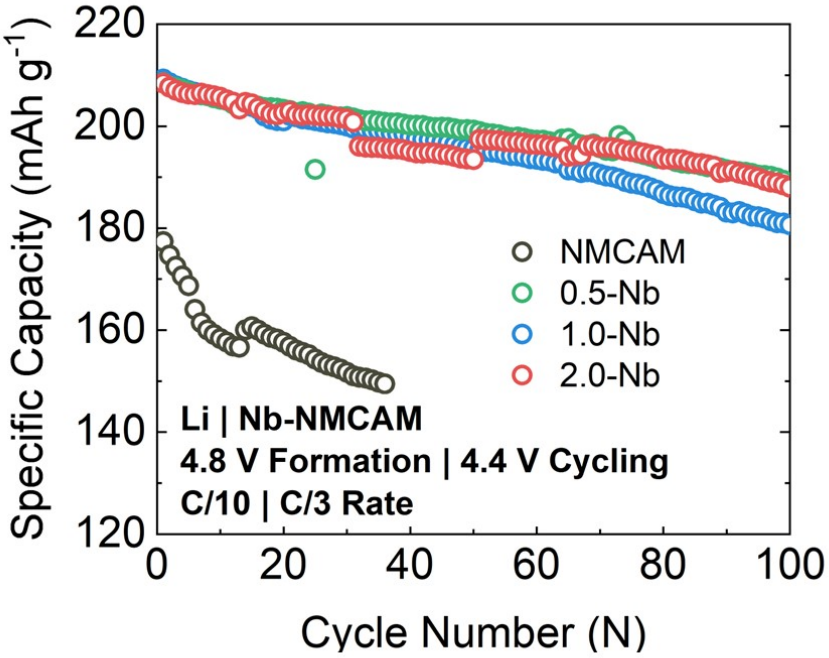

Figure S30. Electrochemical performances of Nb-NMCAM samples cycled under a 4.8 V CC-CV formation at C/10 rate for two cycles, followed by C/3 rate cycling at 4.4 V cutoff.

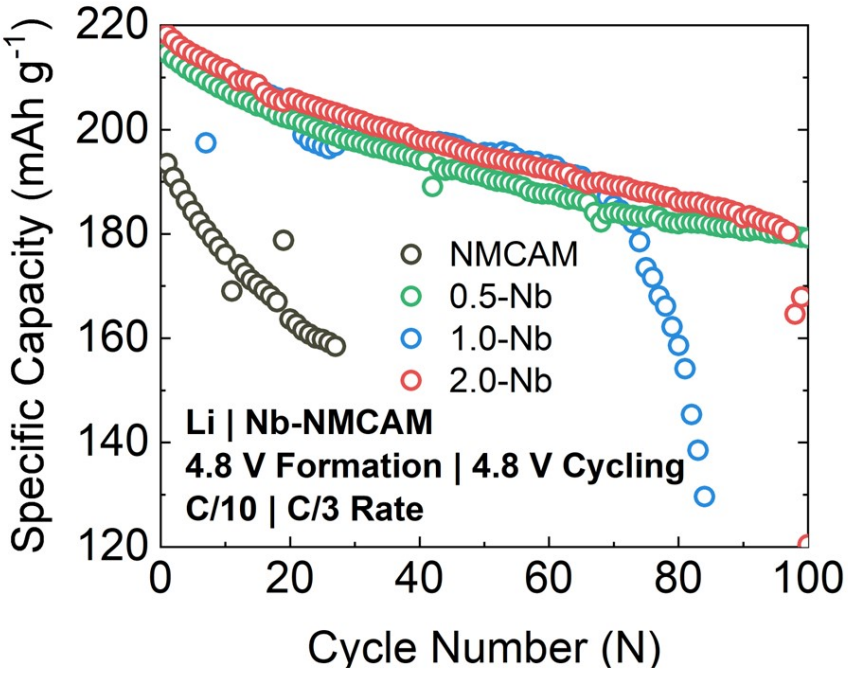

Figure S31. Electrochemical performances of Nb-NMCAM samples cycled under a 4.8 V CC-CV formation at C/10 rate for two cycles, followed by C/3 rate cycling at a 4.8 V cutoff.

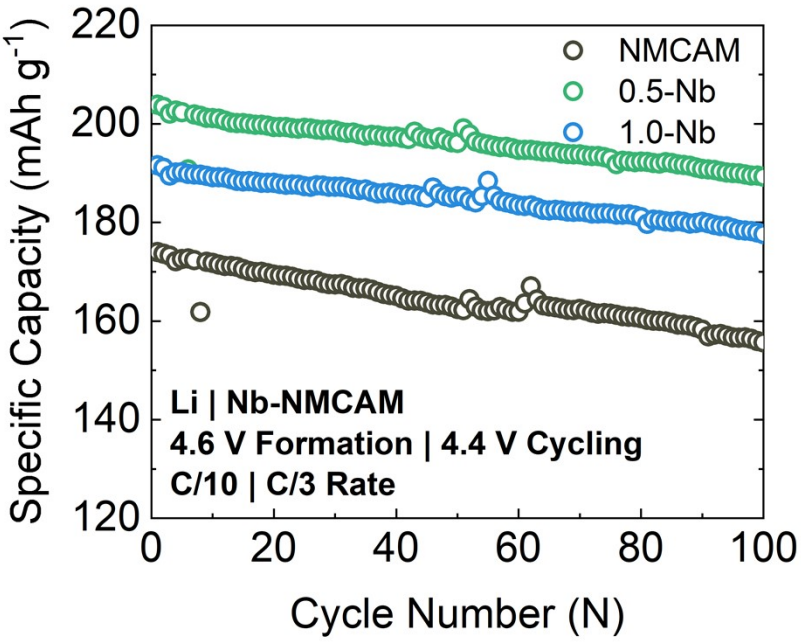

Figure S32. Electrochemical performances of Nb-NMCAM samples cycled under a 4.6 V CC-CV formation at C/10 rate for two cycles, followed by C/3 rate cycling at 4.4 V cutoff.

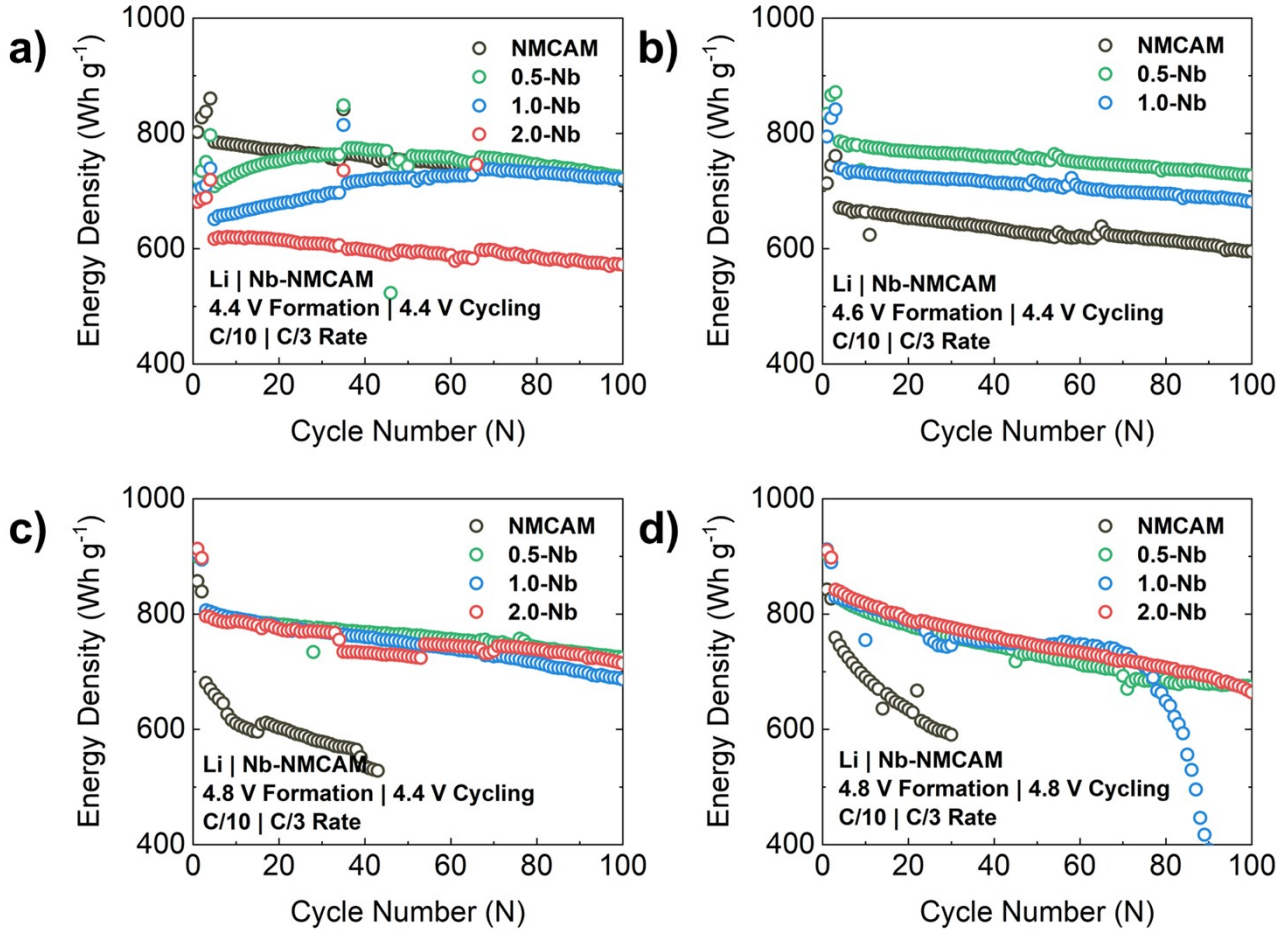

Figure S33. Specific energy vs. cycle number of NMCAM, 0.5-Nb, 1.0-Nb, and 2.0-Nb half cells cycled at (a) 4.4 V cutoff for C/10 formation and C/3 cycling, (b) 4.6 V cutoff for C/10 formation and 4.4 V cutoff for C/3 cycling, (c) 4.8 V cutoff for C/10 formation and 4.4 V cutoff for C/3 cycling, and (c) 4.8 V cutoff for C/10 formation and C/3 cycling.

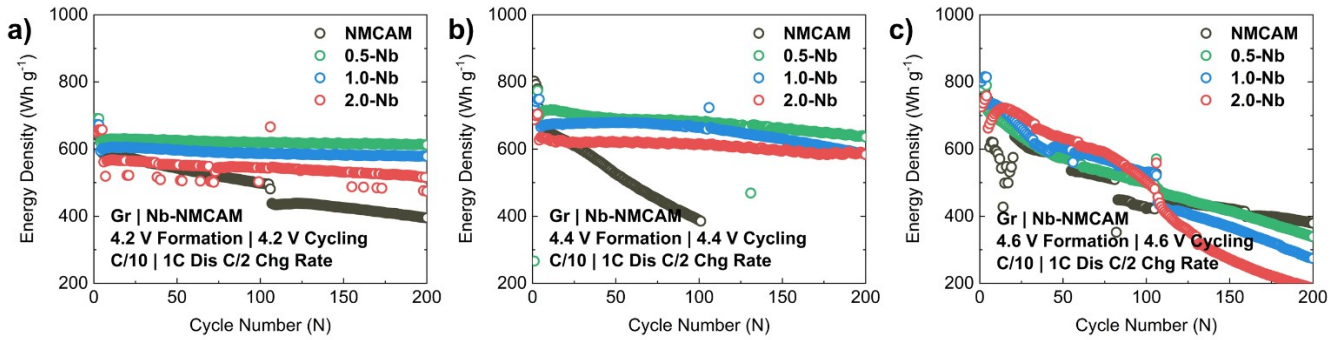

Figure S34. Specific energy vs. cycle number of NMCAM, 0.5-Nb, 1.0-Nb, and 2.0-Nb full cells cycled at (a) 4.2 V cutoff, (b) 4.4 V cutoff, and (c) 4.6 V cutoff.

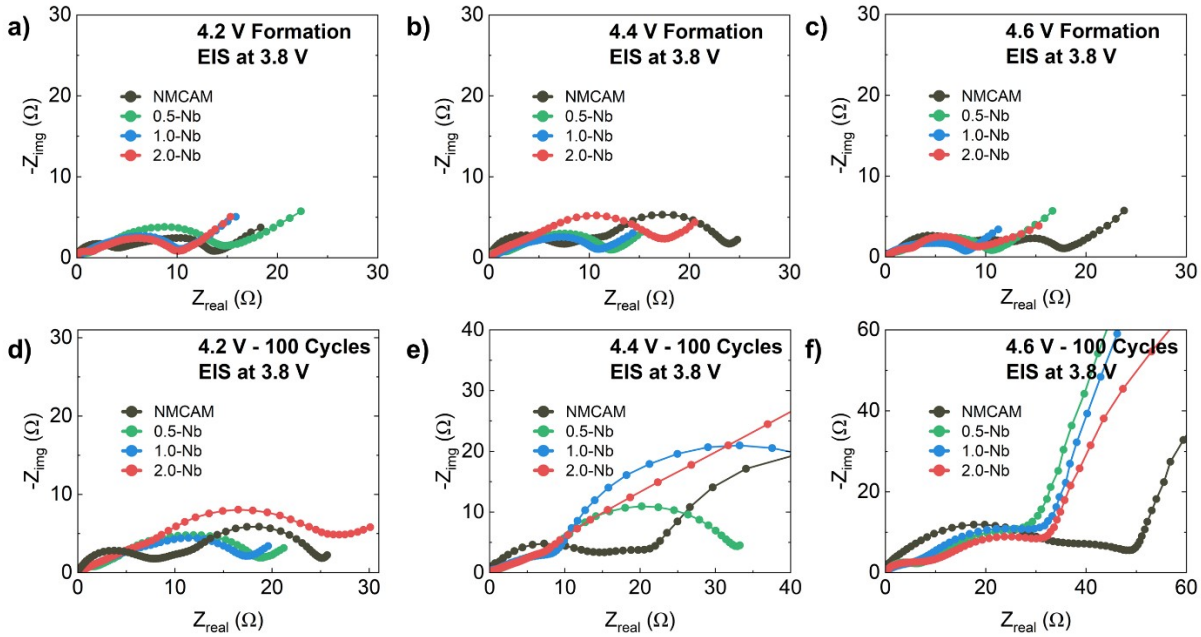

Figure S35. Nyquist plots of NMCAM and Nb-modified NMCAM full cells after three C/10 formation cycles, employing a (a) 4.2 V cutoff, (b) 4.4 V cutoff, and (c) 4.6 V cutoff, and after 100 cycles at C/2 charge - 1 C discharge, employing a (a) 4.2 V cutoff, (b) 4.4 V cutoff, and (c) 4.6 V cutoff.

Table S1. Summary of Rietveld refinement results for the Nb-modified NMCAM samples

	ex Li	FWHM (003)	FWHM (104)	a (Å)	c (Å)	Li^{+} / Ni^{2+}	X^2	R_w
Baseline	1%	0.203	0.270	2.8731	14.1970	0.956 / 0.044	8.97	8.85
0.5-Nb	5.5%	0.213	0.290	2.8725	14.2006	0.963 / 0.037	7.30	8.01
1.0-Nb	1%	0.280	0.360	2.8731	14.1897	0.926 / 0.074	6.74	8.55
1.0-Nb	4%	0.240	0.360	2.8727	14.1965	0.953 / 0.047	6.01	8.02
1.0-Nb	7%	0.238	0.325	2.8726	14.1974	0.954 / 0.046	7.60	8.15
2.0-Nb	1%	0.320	0.400	2.8740	14.1787	0.907 / 0.093	8.38	9.46
2.0-Nb	7%	0.320	0.400	2.8729	14.1887	0.926 / 0.074	7.31	8.81
2.0-Nb	10%	0.288	0.369	2.8726	14.1924	0.943 / 0.057	7.81	8.35